IEEE Open Journal of
Power Electronics

Received 27 May 2024; revised 10 July 2024; accepted 13 July 2024. Date of publication 16 July 2024;
date of current version 24 July 2024. The review of this article was arranged by Associate Editor Nitin Agarwal.

Digital Object Identifier 10.1109/OJPEL.2024.3429412

Development of a Generalized Multilevel SVM and Capacitor Voltage Balancing Strategy for Multiphase Three-Level NPC Converters

MAHDI HOMAEINEZHAD (Graduate Student Member, IEEE) AND OMID BEIK (Senior Member, IEEE)

Department of Electrical Engineering, Colorado School of Mines, Golden, CO 80401 USA

CORRESPONDING AUTHOR: MAHDI HOMAEINEZHAD (e-mail: mahdihomaeinezhad@mines.edu)

ABSTRACT This paper proposes a generalized space vector modulation (SVM) strategy for 3-level neutral-point-clamped (NPC) converters. The proposed strategy, here referred to as multiphase 3-level SVM (MP3L-SVM), is developed as a generic modulation technique applicable for 3-level NPC converters with any number of phases, while for showcasing in this paper the proposed MP3L-SVM is applied to a wind turbine with a direct drive multiphase permanent magnet generator (PMG) whose output is rectified using a 3-level NPC converter before connection to a high-voltage DC (HVDC) grid. A key challenge in 3-level NPC converters is maintaining a balanced voltage across the HVDC-link capacitors, particularly at low speeds. To address this issue, the paper integrates the proposed MP3L-SVM strategy with a voltage balancing algorithm (VBA), which mitigates capacitor voltage imbalances by choosing the three nearest switching states that result in minimal energy deviations across the capacitors. The paper discusses the mathematical modeling of a multiphase PMG interfaced to a 3-level NPC and derives generalized models that govern the proposed strategy based on a visual space vector diagram (SVD). Analytical models are validated through simulations across various 3-level NPC configurations, including 3-phase, 6-phase, and 9-phase NPC converters. Further, the analytical models and simulation results are validated by test results from a scaled-down laboratory prototype 3-level NPC converter that has been prototyped in-house.

INDEX TERMS Multilevel converter, multiphase converter, NPC converter, SVM, voltage balancing, wind turbine.

I. INTRODUCTION

Multiphase multilevel converters offer enhanced characteristics compared to conventional 3-phase multilevel converters, such as improved control [1], [2], increased power density [3], [4], better fault tolerance [5], enhanced reliability, and increased energy accessibility [2], [6]. Furthermore, in applications where different generating units are connected, these converters can play an important role in maximizing power transfer from generation to the grid [7]. Among the variety of multilevel topologies such as neutral point clamped (NPC) converters, cascaded H-bridge (CHB) converters, and flying capacitor (FC) converters, and the topologies derived from these, the NPC topology is one of the most popular owing to its simple topology, relatively low number of switches and capacitors, small-sized filters to eliminate harmonics, ability to better regulate reactive power, and generally lower cost [8]. Different studies have been conducted for these converters, e.g., the reduced capacitor in NPC leads to enhanced reliability due to high failure rate of capacitors [9]; the NPC single input requirement reduces the number of component counts [10]; and the voltage balancing is facilitated in NPC due to clamping feature [11]. Different control methods have been developed for multilevel converters, such as conventional pulse width modulation (PWM) [12], selected harmonics elimination technique (SHE) [13], sliding mode control (SMC) approach [14], and other methods that are derived from these techniques [15], [16], [17], [18], [19]. Among these methods the space vector modulation (SVM) has been increasingly used for multilevel converters, particularly where the current harmonics are small while obtaining output voltage as large as possible is of interest [20], [21], [22]. However, for multiphase converters there are a limited number of studies

related to control and modulation techniques. The authors in [23] introduced an SVM method for a 5-phase 3-level NPC converter, which is split into two *d-q* components: one for the fundamental harmonic, $d_1 - q_1$, and another for the third harmonic, $d_3 - q_3$. This technique effectively eliminates the third harmonic of the voltage by manipulating the voltage vector in the $d_3 - q_3$ vector space to be zero, consequently resulting in a sinusoidal output voltage. They employed a vector space decomposition method to separate the inverter states and defined a decagon region to locate the reference voltage vectors. In [24] a similar SVM technique for a 5-phase 3-level NPC converter was explored without resorting to two *d-q* components, with a subsequent comparison between SVM and PWM techniques regarding total harmonic distortion (THD) of the phase voltage, harmonic distortion of phase voltage components in mutually perpendicular planes, and common mode voltage harmonic distortion. However, the conclusions drawn in reference [24] are confined to the 5-phase 3-level converter and lack generalization, i.e., they cannot be applied to other multilevel converters with different phase numbers. In [25] a SVM technique for an asymmetrical 6-phase 3-level NPC converter is proposed, relying on vector space decomposition to establish asymmetrical sectors and subsectors. However, this method presents challenges in calculating higher numbers of levels and cannot be applied to converters with different phase configurations. Expanding on the work in [24] the authors in [26] focus on developing an SVM algorithm for a 7-phase 3-level NPC converter using vector space decomposition and analyzing multidimensional space vector projections in mutually orthogonal planes. This simplifies calculations and reduces the number of switching states, yielding comparable performance to conventional PWM techniques. In [27] a feedforward SVM approach is proposed for multiphase and multilevel converters based on analytical modeling. This method relies on measuring the DC voltages of the multilevel converter to generate switching signals, ensuring the averaged output waveforms align with the desired reference. Authors in [28] investigate a PWM technique equivalent to SVM for a 5-phase 5-level converter and provide a comparative analysis between the two methods. However, a generalized approach for multiphase 3-level SVM techniques is absent in current literature. Existing techniques commonly follow similar procedures for dwell time calculations, involving transformation and projection of reference voltages onto α-β or *d-q* planes, defining sectors based on these transformations, optimizing switching sequences, and calculating dwell times using volt-time equations of the system.

This paper introduces a hierarchical calculation approach, establishing a framework for applying a SVM technique to multiphase 3-level NPC converters with any number of phases. The authors have previously discussed the proposed framework in [29], [30], [31], [32], covering various applications and introducing the fundamental calculations and visualization concepts. In previous works by the authors, fundamental calculations of SVM were initially provided to introduce the generalized SVM concept. Subsequently, various benchmark systems were presented to implement the multiphase NPC converter, controlled by generalized SVM, to enhance overall system performance. Simulation studies were conducted to evaluate the proposed strategy's performance for systems with an even number of phases. However, systems with an odd number of phases, such as symmetrical and asymmetrical six-phase systems commonly used in various applications, were not addressed. In the literature, there are studies that only consider one configuration e.g., three-phase [12], five-phase [24], or seven-phase [26]. Moreover, the Space Vector Diagram (SVD) concept was introduced only for symmetrical systems both in the previous work of the authors and in the literature, which is not always applicable since asymmetrical six-phase systems can also be employed. Furthermore, previous simulation studies by the authors did not include AC side evaluations, such as the terminal voltage and current of the generator. This research aims to address these gaps by conducting detailed simulation and experimental studies for both even and odd-numbered phase systems. The performance of the proposed strategy is evaluated using a scaled-down real-world experimental test setup. Additionally, this paper examines how the proposed modulation strategy balances the voltage across the converter capacitors and compares the results of the widely used PWM strategy with the proposed control strategy. Although this paper integrates the generalized SVM with a voltage balancing algorithm to improve system performance, it requires more calculations compared to previous works. Table 1 summarizes the significant improvements of this research compared to the authors' previous works.

TABLE 1. Summary of Improvements

Existing literature	Gaps	Paper's contribution
Limited number of phases considered, e.g. 3-ph [12], 5-ph [24], 6-ph [25], or 7-phase [26]	No generalized SVM approach for all phase numbers	A generalized SVM developed that is applicable to any number of phases, odd and even.
Limited number of phases considered for creating SVD, e.g. 3-ph [12]	No generalized SVD for all phase numbers and configurations	Development of SVD for asymmetrical configurations
Limited number of phases and levels are considered, e.g. 3-ph 5-level [36]	No generalized VBA algorithm and integration for all phase numbers	Voltage balancing studies
Limited number of phases considered, e.g. 3-ph [12], 5-ph [24], 6-ph [25], or 7-phase [26]	No generalized experimental studies for all phase numbers	Experimental studies for 3-ph, 6-ph, and 9-ph configurations
Limited number of phases considered, e.g. 3-ph [12], 5-ph [24], 6-ph [25], or 7-phase [26].	No comparison studies for different number of phases	AC side voltage and current evaluation for 3-ph, 6-ph, and 9-ph (simulation and experimental studies)

The proposed modulation strategy, here referred to as multiphase 3-level SVM (MP3L-SVM), addresses the inherent challenges of modulation technique including identifying

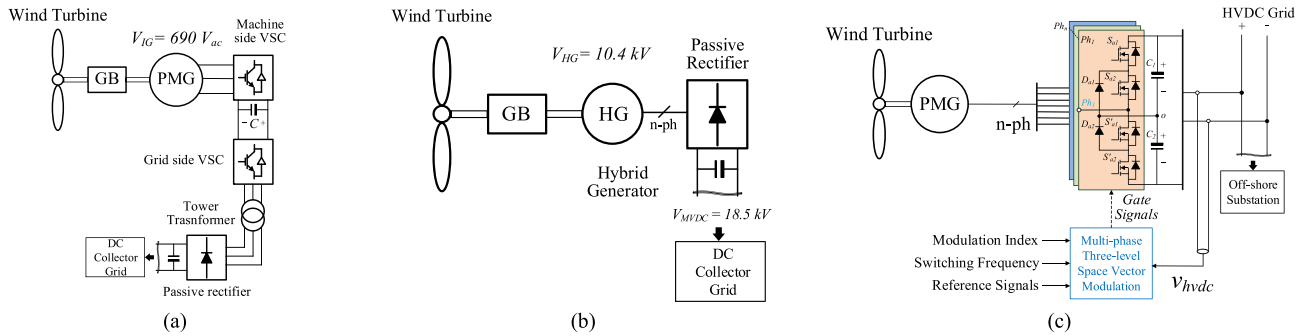

FIGURE 1. (a) Wind turbine conversion in Walney wind farm. (b) High-voltage wind turbine conversion system connected to a DC collector grid proposed in [5], [6], [7]. (c) Wind turbine conversion system overview with multiphase 3-level NPC converter.

suitable switching states for the multiphase 3-level NPC converters while mitigating potential short-circuit occurrences. It leverages the SVD to determine switching states and synthesize a reference voltage. The paper integrates a voltage balancing algorithm (VBA) with the MPML-SVM to address voltage imbalance issues across the high-voltage DC (HVDC) capacitors. Analytical models of multiphase systems and MP3L-SVM are derived and verified via simulation studies for a 3-level NPC converter with 3-, 6-, and 9-phases. Further, a laboratory prototype multiphase 3-level NPC converter configurable for 3-ph, 6-ph, and 9-ph has been built and tested to confirm the analytical and simulation results.

The modulation strategy is formulated to generalize the modulation process across any number of phases, providing a versatile solution adaptable to different system requirements without the need for reconfiguration. An innovative integration of a voltage balancing algorithm (VBA) is included to address capacitor voltage imbalances, which is critical for stable and efficient converter operation. Traditional methods, as discussed in [23], [24], [25] often require intricate vector transformations and a detailed understanding of the converter topology to be implemented effectively. In contrast, the SVM process is simplified by the MP3L-SVM using a hierarchical approach to determine switching states directly from the space vector diagram, reducing computational complexity and enhancing real-time applicability. Previous approaches are generally optimized for a fixed number of phases and levels, as seen in [23] for a five-phase system and [26] for a seven-phase system. This limitation is not shared by MP3L-SVM, which offers scalability to any number of phases, a significant advantage in systems requiring customization or future upgrades. Furthermore, the experimental test setup of this research utilizes a modified generator that can be configured as a three-, six-, or nine-phase system to assess performance, a unique characteristic of this paper.

II. BENCHMARK WIND TURBINE AND MULTIPHASE SYSTEMS

To provide a practical application to real-world scenarios, this paper selects the Siemens wind turbine model SWT-3.6-107 as a benchmark system [3]. This wind turbine is used in Walney, one of the world's largest offshore wind farms, situated in the Irish Sea off the coast of the U.K.. The benchmark wind turbine incorporates a 3-phase induction machine (IM) with a rating of 690 V and 3.6 MW, along with two fully rated conventional 2-level back-to-back voltage source converters (VSCs), and step-up transformer that connects the wind turbine to a 33 kV AC grid as shown in Fig. 1(a).

In an effort to introduce high-voltage conversion systems that facilitate connection of wind turbines to a DC collector grid the authors in [5], [6], [7] proposed a multiphase high-voltage hybrid generator design interfaced to a passive rectifier as shown in Fig. 1(b). In their topology the active rectification stage has been eliminated and the entire control functionality has been shifted to the hybrid generator. Although this will provide control on the wind turbine output voltage, the current cannot be fully controlled over the entire region of operation as there are no active switches. Additionally, given the uncontrolled nature of passive rectifier, when the wind turbines are connected in parallel any disparity among the output voltage of wind turbines will force the rectifier stage to turn-off hence putting the wind turbine out of operation. An improvement to the scheme in Fig. 1(b) would be to use an active rectifier. However, as the power electronics switches are not available at high voltages a 2-level topology would not be suitable, thus a 3-level NPC converter topology may be used as shown in Fig. 1(c).

Note, since the NPC converter provides an active control over the wind turbine output the hybrid generator can be replaced by a commonly used high-voltage permanent magnet generator (PMG), hence making the conversion system simplified. The system specifications, including voltage, power, and speed for the scheme in Fig. 1(c) are adopted from the scheme presented in Fig. 1(b) [5], and presented in Table 2. Specifically, one of the features of the conversion system that the authors in [5] have designed is a machine with multiphase winding that results in improved power-density, efficiency, reliability, and fault tolerance [5]. Specifically, in multiphase (greater than 3-phase) winding as the number of phases increases, the machine's back-EMF, and consequently the rectified voltage at the output of power electronics interface increases due to improved winding factor [33], [34]. Increasing the number of phases reduces phase-shifts between voltages and currents in HVDC systems, resulting in lower

TABLE 2. Wind Turbine System Specifications [3]

Wind Turbine model	Siemens SWT-3.6-107
Cut-in wind velocity (m/s)	4
Rated velocity (m/s)	14
Cut-out wind velocity (m/s)	25
hybrid generator rated power (MW)	0.1 – 3.6 @ (cut-in – rated velocity)
Rotor speed (RPM)	169 – 600 @ (cut-in – rated velocity)
9-phase per-phase RMS back-EMF (kV)	2.89 – 10.29 @ (cut-in – rated velocity)

TABLE 3. Multiphase Winding and Rectified DC Characteristics [31]

n-ph	Winding coil		Back-EMF		Rectified HVDC voltage	
	Turns	Winding factor	RMS (kV)	Increase from 3-ph (%)	Average (kV)	Ripple (%)
3	n_c	1	10	-	23.4	15.5
5	$5/3\, n_c$	1.0292	10.29	2.92	26.6	5.43
7	$7/3\, n_c$	1.0383	10.38	3.83	27.6	2.76
9	$3n_c$	1.042	10.42	4.20	28	1.66

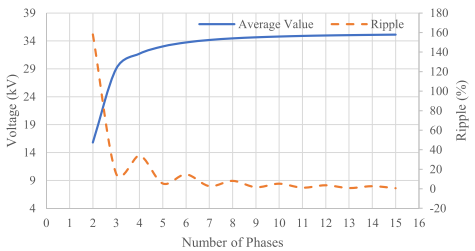

FIGURE 2. Rectified average voltage and ripple factor of multiphase systems.

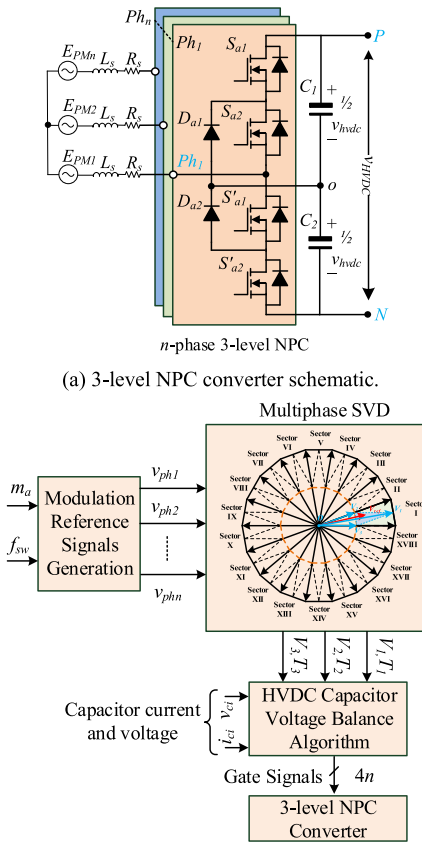

(a) 3-level NPC converter schematic.

(b) MP3L-SVM switching strategy overview.

FIGURE 3. Proposed modulation strategy and 3-level NPC. (a) 3-level NPC converter schematic. (b) MP3L-SVM switching strategy overview.

ripple in rectified voltage and current. Table 3 compares the back-EMF and rectified VDC voltage for a machine with different number of phases. Note, for a multiphase machine an odd number of phases is selected as compared to even phase numbers it results in further gains in average voltage and reduced ripple [29]. Additionally, the gains for the phase numbers beyond the 9-phase system reduce, as shown in Fig. 2. Thus, the higher phase numbers are usually not considered, unless the application has such requirements [30].

III. MULTIPHASE 3-LEVEL SVM

Fig. 3(a) shows a schematic view of an n-phase 3-level NPC converter that interfaces the PMG in the benchmark wind turbine to the HVDC grid. The generator is modelled as PMG back-EMF (E_{PMi}) in series with R_s, and L_s (per-phase resistance and inductance). The 3-level NPC converter has 4 switches per leg, while three switching states based on ON (1) and OFF (0) state of the switches is realized. This results to an output phase voltage ($v_{Ph1-to-N}$ & $v_{Ph1-to-G}$) with three levels, i.e., zero, $\frac{1}{2}v_{HVDC}$, and v_{HVDC}. For an n-phase, 3-level converter the total number of switching states (n_{sws}), switches (n_{sw}), diodes (n_d), and HVDC capacitors (n_c) are:

$$n_{sws} = 3^n - n_{co},\ n = 2k+1,\ k = 1,\ 2,\ \ldots$$

$$n_{sw} = 4n,\ \ n_d = 2n,\ n_c = 2 \tag{1}$$

where, n_{co} is the number of common switching states that they result in zero voltage or the same output voltage.

A. SWITCHING STRATEGY

The switching strategy for the proposed MP3L-SVM is illustrated in Fig. 3(b). Given a desired modulation index (m_a), and the fundamental output frequency (f_0), the n-phase reference modulation signals (v_{ph1}, v_{ph2}, … v_{phn}) are generated as in (2). The amplitude of the phase voltage signal, is defined by the modulation index and HVDC voltage, while a sinusoidal at a frequency of f_0, and the phase shift of ($\frac{2\pi(i-1)}{n}$) defines its angle:

$$v_{ph_i} = m_a.V_{HVDC}.\sin\left(2\pi f_o t - \frac{2\pi\,(i-1)}{n}\right)$$

$$i = 1,\ 2, \ldots,\ n;\ \ and\ m_a = \frac{\left|\vec{V}_{ref}\right|}{V_{HVDC}} \tag{2}$$

where, $|\vec{V}_{ref}|$ is the amplitude of a reference voltage calculated based on the n-phase reference modulation signals.

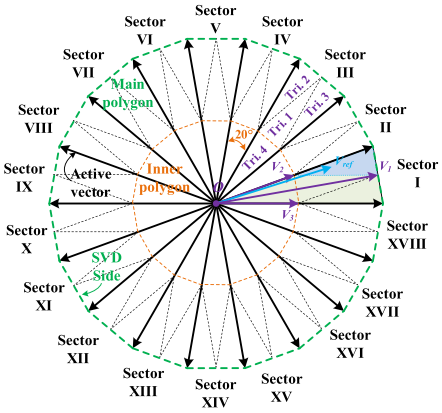

FIGURE 4. 9-phase 3-level SVD and its characteristics.

The multiphase modulation signals are transformed to 2-axis signals (v_α, v_β) using multiphase-to-$\alpha\beta$ transformation [32]:

$$\begin{bmatrix} V_\alpha \\ V_\beta \end{bmatrix} = \frac{2}{n} \begin{bmatrix} 1 & \cos\frac{2\pi}{n} & \cos\frac{4\pi}{n} & \cdots & \cos\frac{2(n-1)\pi}{n} \\ 0 & -\sin\frac{2\pi}{n} & -\sin\frac{4\pi}{n} & \cdots & -\sin\frac{2(n-1)\pi}{n} \end{bmatrix} \times \begin{bmatrix} v_{ph1} \\ v_{ph2} \\ \vdots \\ v_{phn} \end{bmatrix} \tag{3}$$

Therefore, a reference voltage vector $\vec{V}_{ref}$ is calculated as:

$$\begin{aligned} \vec{V}_{ref} &= V_\alpha + jV_\beta \\ |V_{ref}| &= \sqrt{{V_\alpha}^2 + {V_\beta}^2} \\ \theta &= \tan^{-1}\left(\frac{V_\beta}{V_\alpha}\right) \end{aligned} \tag{4}$$

where, θ is the reference voltage angle.

Given the reference voltage the switching states for the MP3L-SVM are realized in process as follows:

1) An SVD is formed, as exemplified for a 9-phase 3-level converter in Fig. 4. For an n-phase converter, the SVD comprises $2n$ active vectors spanning 360°, with each vector phase-shifted by $(\frac{360°}{2n})$ from its adjacent counterpart. These active vectors connect to create a polygon, denoted as the main polygon in Fig. 4, with $2n$ sides. The polygon is further divided into $2n$ sectors, delineated by two adjacent active vectors and one main polygon side. In the case of the 9-phase 3-level converter, there are 18 active vectors, each with a 20° phase shift from the next, thus forming an 18-sided main polygon. Consequently, there are 18 sectors, labeled as Sector I to Sector XVIII, with Sector I highlighted in green in Fig. 4. For an m-level converter, multiple polygons are formed concentrically within one another. The amplitude (length) of active vectors in each polygon corresponds to the voltage level defined in (1). In the illustrated 3-level converter in Fig. 4, two polygons exist, where the amplitude of active vectors for the main polygon is V_{HVDC}, while it is $\frac{1}{2}V_{HVDC}$ for the active vectors in the inner polygon. Notably, the number of polygons depends on the converter's levels and remains independent of the number of phases. For the 3-level converter, each sector is divided into four triangles, as indicated by the dotted lines in Fig. 4. Each triangle vertex represents a voltage vector, defining a specific switching state for the 3-level NPC converter. Each vector possesses an amplitude, an angle, and an associated switching time, referred to as dwell time, which specify the duration within the switching period (T_s).
2) The reference voltage, given its amplitude ($|\vec{V}_{ref}|$) and angle (θ), is laid inside the SVD. For the 9-phase 3-level converter the reference voltage ($\vec{V}_{ref}$), in this example, is laid in Sector I in a triangle highlighted in blue in Fig. 4. The reference voltage may be synthesized based on the three nearest vectors ($\vec{V}_1$, $\vec{V}_2$, $\vec{V}_3$) and their dwell times (T_1, T_2, T_3) using the volt-second equilibrium [31]:
$$\begin{aligned} \vec{V}_1 T_1 + \vec{V}_2 T_2 + \vec{V}_3 T_3 &= \vec{V}_{ref} T_s \\ T_1 + T_2 + T_3 &= T_s \end{aligned} \tag{5}$$
The switching states and their dwell times obtained from (5) are applied to the 3-level NPC converter in a repetitive switching period. For any combination of phases and converter levels, the synthesis of the reference voltage necessitates only three voltage vectors. It's important to note that the reference voltage can be synthesized using any three voltage vectors within the SVD. However, this approach can introduce higher harmonic distortion and increased losses.
3) For an n-phase and 3-level converter:
$$\begin{aligned} &\left|\vec{V}_1\right| e^{j\theta_1} T_1 + \left|\vec{V}_2\right| e^{j\theta_2} T_2 + \left|\vec{V}_3\right| e^{j\theta_3} T_3 = \vec{V}_{ref} e^{j\theta} T_s \\ &0 \le \theta_1 \le \frac{\pi}{n},\ 0 \le \theta_2 \le \frac{\pi}{n},\ 0 \le \theta_3 \le \frac{\pi}{n},\ 0 \le \theta \le \frac{\pi}{n} \end{aligned} \tag{6}$$
where, θ_1, θ_2, θ_3 are the angle for vectors $\vec{V}_1$, $\vec{V}_2$, $\vec{V}_3$, respectively.

As denoted by the range of angles in (6), the reference voltage, if laid in any sector, is shifted to the first sector, Sector I, where its angle is between zero and $\frac{\pi}{n}$. This simplifies the calculation and facilitates development of a general framework for an MP3L-SVM with any number of phases and levels. Once the reference voltage vector is in the first sector, depending on the number of triangles in Sector I, i.e., converter levels, the three nearest voltage vectors are selected and replaced in (6), whereby separating the equation into real and imaginary parts and solving for dwell times, T_1, T_2, and T_3 are obtained.

B. GENERALIZED DWELL TIMES

For n-phase 3-level SVM the dwell times are listed in Table 4. For 3-level converters the SVD consists of two polygons

TABLE 4. Generalized Dwell Times for an N-Phase 3-Level MP3L-SVM [33]

Dwell Times		Expression
Tri. 1	T_1	$T_s(1+\frac{\sqrt{3}V_{ref}(sin(\theta-\frac{\pi}{n})-\sin(\theta))}{V_{DC}\sin(\frac{\pi}{n})})$
	T_2	$\frac{\sqrt{3}T_sV_{ref}\sin(\theta)}{V_{DC}\sin(\frac{\pi}{n})}$
	T_3	$\frac{-\sqrt{3}T_sV_{ref}\sin(\theta-\frac{\pi}{n})}{V_{DC}\sin(\frac{\pi}{n})}$
Tri. 2	T_1	$\frac{3T_s(V_{DC}\sin(\frac{\pi}{2n})-V_{ref}(3\sin(\theta-\frac{\pi}{2n})-\sqrt{3}\sin(\theta-\frac{\pi}{n}))}{V_{DC}(6\sin(\frac{\pi}{2n})-\sqrt{3}\sin(\frac{\pi}{n}))})$
	T_2	$\frac{-\sqrt{3}T_s(V_{DC}\sin(\frac{\pi}{n})+3V_{ref}(sin(\theta)-\sin(\theta-\frac{\pi}{n}))}{V_{DC}(6\sin(\frac{\pi}{2n})-\sqrt{3}\sin(\frac{\pi}{n}))}$
	T_3	$\frac{3T_s(V_{DC}\sin(\frac{\pi}{2n})+V_{ref}(3\sin(\theta-\frac{\pi}{2n})-\sqrt{3}\sin(\theta))}{V_{DC}(6\sin(\frac{\pi}{2n})-\sqrt{3}\sin(\frac{\pi}{n}))})$

where each sector is divided into four triangles, (Tri. 1, Tri. 2, Tri. 3, and Tri. 4) as seen from Fig. 4. Therefore, the reference voltage, once shifted to Sector I, is synthesized based on the triangle in which is lays, hence resulting in different dwell times based on four triangles as listed in Table 4. NPC converters are known for their versatility in both inverter and rectifier operations. However, NPC rectifiers present unique challenges. One such challenge arises from the discrepancies in switching states between rectifiers and inverters. For example, what constitutes a zero-voltage level in an inverter equates to a short-circuit condition in a rectifier. Moreover, in a rectifier, if all switches are turned off, the converter functions as a passive rectifier. In contrast, in an inverter, if all switches are off, the converter effectively shuts down. As a result, the inclusion of emergency shut-down switches becomes imperative for ensuring the safe operation of rectifiers.

One important aspect of the proposed modulation strategy is its applicability to asymmetric configurations, such as the well-known asymmetric six-phase configuration. As mentioned earlier, the calculations remain exactly the same for every configuration and conversion type. However, the input to the equations comes from the SVD. Therefore, the same calculations can be applied to every configuration, but the SVD must be adjusted accordingly. In an asymmetric six-phase configuration, there are two sets of three-phase systems shifted by 30 °C from one another. Thus, the SVD can be realized based on the same analysis: two hexagons with a 30 °C shift between them. Based on this explanation, the realized SVD is shown in Fig. 5(b). It is evident that the SVD is no longer a symmetric shape due to the uneven phase shifts in this system. Fig. 5(a) illustrates how the vectors of this system are positioned relative to each other.

Furthermore, to compare the performance of the proposed modulation strategy with conventional methods such as Sinusoidal PWM (SPWM), the SVDs of both strategies are shown in Fig. 6. Both are designed for a nine-phase configuration. One of the main advancements of MP3L-SVM is better voltage utilization. As seen, the largest reference vector that can be used in SPWM (V_(ref-SPWM)) is the radius of its SVD. However, this vector (V_(ref-SVM)) is larger for the MP3L-SVM method. In other words, for the same input, SVM

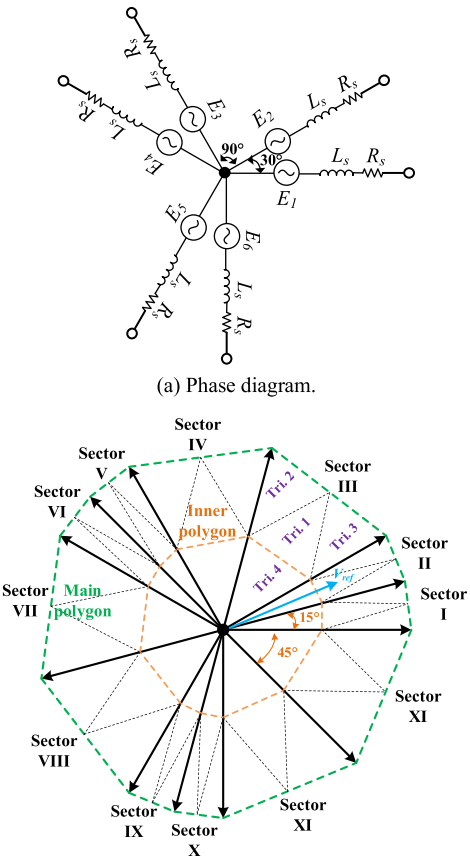

(a) Phase diagram.

(b) Space vector diagram.

FIGURE 5. Asymmetric six-phase system phase diagram and SVD. (a) Phase diagram. (b) Space vector diagram.

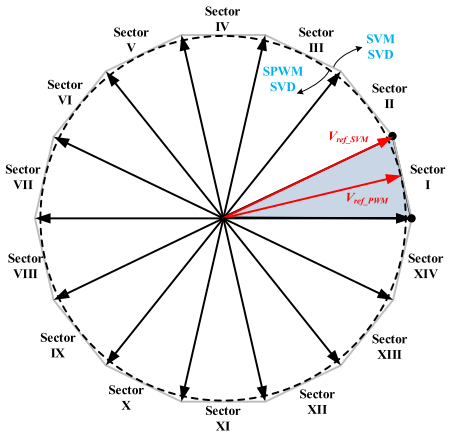

FIGURE 6. Space vector diagram for MP3L-SVM versus SPWM.

can result in a higher output voltage compared to SPWM. Additionally, simulation studies show that for a multiphase converter, the total harmonic distortion (THD) of the output voltage is between 3-10% for SVM and 5-15% for SPWM. SVM can potentially offer lower THD compared to standard PWM because it maximizes DC bus utilization and provides a more uniform distribution of the switching vectors throughout the switching cycle, leading to smoother voltage transitions

and less harmonic generation. Both strategies can achieve reduced THD with higher switching frequencies. However, SVM has an improved THD at comparable frequencies due to its more efficient vector utilization. Nonetheless, SVM is generally more complex to implement than PWM, as it requires more intricate calculations for determining the switching times and sequences. PWM, especially simple SPWM, is easier to implement but might not optimize the DC bus voltage as efficiently.

For multiphase systems that can be built based on multiple three-phase systems, such as six-phase and nine-phase systems, MP3L-SVM is the most optimized strategy to use. A straightforward approach is to use multiple sets of three-phase strategies to achieve multiphase configurations. However, this method presents several difficulties. One major disadvantage is the synchronization process between multiple sets of three-phase configurations. To obtain the desired results, multiple systems must be introduced, and multiple constraints must be implemented to create switching states for each set. Additionally, as the number of phases increases, such as in a nine-phase system, optimizing the best switching states becomes more challenging. Considering the difference between switching states of an inverter and a rectifier, this strategy fails to generalize for both operation modes. Furthermore, in rectifier mode, switching states are very sensitive and can result in short circuits in the system. Introducing multiple three-phase systems makes it harder to prevent switching overlaps and short circuits. In contrast, MP3L-SVM addresses these challenges within its fundamental concept, SVD, and at each step, it selects the most optimized switching state and checks the best one for voltages across the capacitors.

C. VOLTAGE BALANCING ALGORITHM

Assuming two identical HVDC-link capacitors, the total energy of them can be calculated by (7).

$$E = \frac{1}{2}\left(C_1 {V_{C1}}^2 + C_2 {V_{C2}}^2\right) \rightarrow E = \frac{1}{2}\left(C_1 \frac{{V_{DC}}^2}{4} + C_2 \frac{{V_{DC}}^2}{4}\right) \tag{7}$$

According to the definition of voltage deviation for the capacitors, a cost function can be realized, and the ultimate purpose of this method is to minimize the cost function. In order to do so, the derivative of the cost function should be equal or less than zero. Equation (7) is denoted as the "minimum energy property" [35], and it serves as the foundation for achieving HVDC-link capacitor voltage balancing. During regular operation, the HVDC-link capacitor voltage tends to deviate from its intended value, which is $\frac{1}{2}v_{DC}$ for a 3-level NPC converter. As a result, the objective is to minimize this deviation in order to achieve the desired voltage balance. Considering all [36]:

$$J = \frac{1}{2}C\left[\left(V_{C1} - \frac{V_{DC}}{2}\right)^2 + \left(V_{C2} - \frac{V_{DC}}{2}\right)^2\right]$$

$$\overset{yields}{\rightarrow} \quad \frac{dJ}{dt} = C_1 \frac{dV_{c1}}{dt}\Delta V_{c1} + C_2 \frac{dV_{c2}}{dt}\Delta V_{c2} \leq 0 \tag{8}$$

TABLE 5. Simulation System Characteristics

Fundamental Frequency	60 Hz
Switching Frequency	6 kHz
HVDC Voltage (rated)	18.5 kV
HVDC Power (rated)	3.6 MW
Generator's Per-phase resistance	0.7 Ω
Generator's Per-phase synchronous inductance	226.91 mH

Applying the average operator over one switching period (T_s) and assuming that the capacitor voltage fluctuations are close to zero in this period, yields:

$$\frac{1}{T_s}\int_{KT_s}^{(k+1)T_s} [i_{C1}\Delta V_{c1} + i_{C2}\Delta V_{c2}] \leq 0$$

$$\rightarrow \ \bar{i}_{C1}\Delta V_{c1} + \bar{i}_{C2}\Delta V_{c2} \leq 0 \tag{9}$$

where $\bar{i}_{C1}$ and $\bar{i}_{C2}$ can be calculated by (8) or measured.

$$\bar{i}_{Ci}(k) = i_{C1}(k,\ S_{x1})\,T_1 + i_{C2}(k,\ S_{x2})\,T_2 + i_{C3}(k,\ S_{x3})\,T_3 \tag{10}$$

where S_{x1}, S_{x2}, and S_{x3} represent the phase switching states corresponding to the switching vectors V_1, V_2, and V_3, respectively.

Equations (9) and (10), corresponding to the switching vectors derived from space vector modulation, are solved simultaneously for all potential device switching states. The converter is then operated in the switching state that yields the smallest energy variation throughout the operation. To provide further clarity, in the analysis of HVDC-link capacitor voltage balancing within one triangular sector, the nearest three switching vectors are considered along with their corresponding switching times, obtained from the MP3L-SVM calculations. The HVDC-link capacitor currents are estimated for all possible switching states using (10). Utilizing the instantaneous values of HVDC-link capacitor currents, the average HVDC-link capacitor current is computed for one sampling interval using (9). Finally, the mathematical condition outlined in (8) is evaluated using the average HVDC-link capacitor current values obtained for device switching states. The switching state that minimizes the energy deviation among all possible switching states is selected and applied to phase A over a sampling interval. This process is iterated for other phases.

IV. SIMULATION RESULTS

In order to validate the performance of the developed MP3L-SVM modulation, simulation studies were conducted on a 3-level NPC converter connected to an HVDC grid in a wind generation system. Simulation specifications are indicated in Table 5.

Fig. 7 illustrates the power-speed curve for the wind turbine. In the startup region, wind velocity remains below the cut-in threshold, and the wind turbine does not generate power. Once the wind velocity surpasses the cut-in point, power generation begins. Within the Maximum Power Point

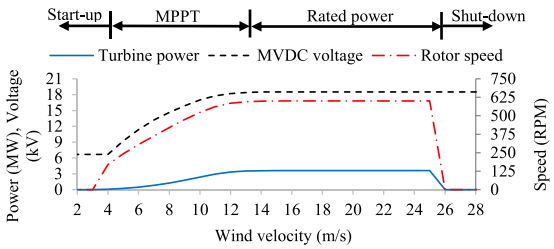

FIGURE 7. **Power-speed characteristics of the wind turbine.**

Tracking (MPPT) region, both output power and HVDC voltage increase to their rated values at a wind velocity of 14 m/s. In the rated power region, the wind turbine consistently operates at its rated values. Beyond the cut-in velocity of 25 m/s, the wind turbine initiates its shutdown process, gradually reducing rotor speed and power output to zero. Throughout this phase, the HVDC voltage remains at the rated value. Subsequently, as wind velocity drops below the cut-out threshold, the wind turbine recommences power generation.

To assess the performance of the proposed MP3L-SVM modulation strategy, three simulation scenarios were selected: i) wind velocity of 10 m/s (PMG power of 1.8 MW), ii) wind velocity of 5 m/s (PMG power of 0.2 MW), and iii) wind velocity of 15 m/s (PMG power of 3.6 MW). Each scenario evaluates three commercially used systems: 3-phase 3-level, 6-phase 3-level, and 9-phase 3-level. It's noteworthy that multiphase systems inherently offer greater fault tolerance. For instance, in a 3-phase generator, if one phase faults, 33.34% of the power is lost, and the remaining phases experience an overload of 50% of their rated value. Conversely, in a 9-phase generator, only 11.11% of the power is lost if one phase is faulty, and the other phases endure a manageable overload of just 13%, a factor already considered in the design process.

Fig. 8(a) depicts the rectified voltage for each system across different scenarios. It's evident that the 3-phase system exhibits the highest ripple and the lowest average HVDC-link voltage, whereas the 9-phase system demonstrates the lowest ripple and the highest output voltage compared to the others. This observation aligns with theoretical principles suggesting that as the number of phases increases, the rectified voltage rises due to enhanced winding factor and improved harmonic content, while the ripple decreases. Employing a generator wound for a higher number of phases than the 3-phase setup reduces the HVDC current for the same application, owing to the increased output voltage. Essentially, for the same output power, an increase in the number of phases leads to a reduction in HVDC current, indicating a decrease in the current flowing through the switching components. These trends are illustrated in Fig. 8(b) and (c), representing HVDC current and power, respectively. Fig. 8 demonstrates that the proposed modulation strategy effectively rectifies the voltage across different scenarios and various numbers of phases. Transitions between scenarios are smooth, and the system remains stable throughout.

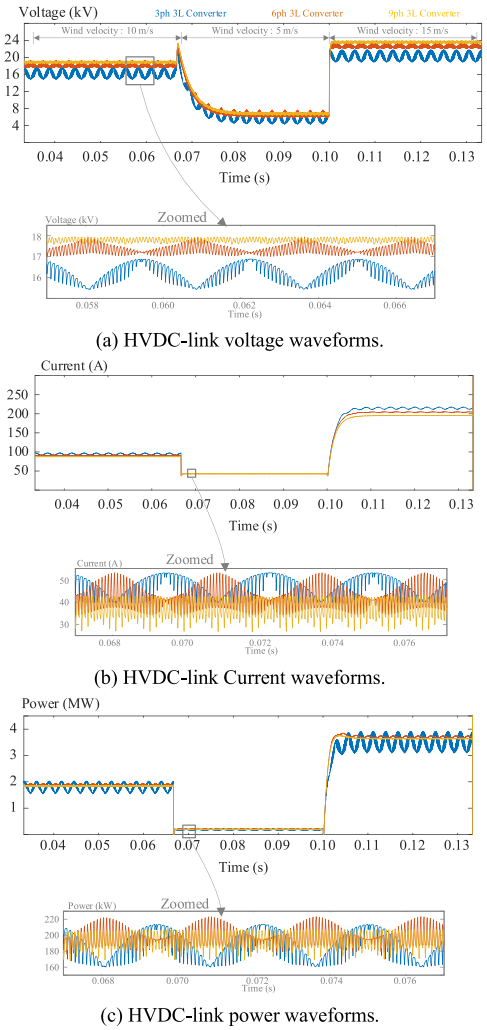

(a) HVDC-link voltage waveforms.

(b) HVDC-link Current waveforms.

(c) HVDC-link power waveforms.

FIGURE 8. **Simulation results for wind velocities of 5, 10, and 15 m/s. (a) HVDC-link voltage waveforms. (b) HVDC-link Current waveforms. (c) HVDC-link power waveforms.**

Fig. 9 shows the per-phase AC voltage at the generator terminal along with the generator's back-EMF. The back-EMF waveforms are nearly pure sinusoids, but the terminal voltage is distorted due to the switching activity. Notably, this distortion decreases as the number of phases increases, as illustrated in the figures. Additionally, Fig. 10 displays the per-phase AC current of the generator. The switching distortion is apparent, and as the number of phases increases, the per-phase current decreases, which aligns with the theoretical discussions presented earlier. Furthermore, to delve into the voltage imbalance issue across the HVDC-link capacitor and evaluate the efficacy of the proposed MP3L-SVM modulation strategy in mitigating this problem, models of 3-phase 3-level and 9-phase 3-level converters are modeled. Each converter is controlled by three approaches: (1) PWM, (2) MP3L-SVM without VBA, and (3) MP3L-SVM with VBA.

Fig. 11(a) depicts the HVDC-link capacitors of the 3-phase system, while Fig. 11(b) illustrates the voltages of the 9-phase system. It is evident that utilizing the PWM

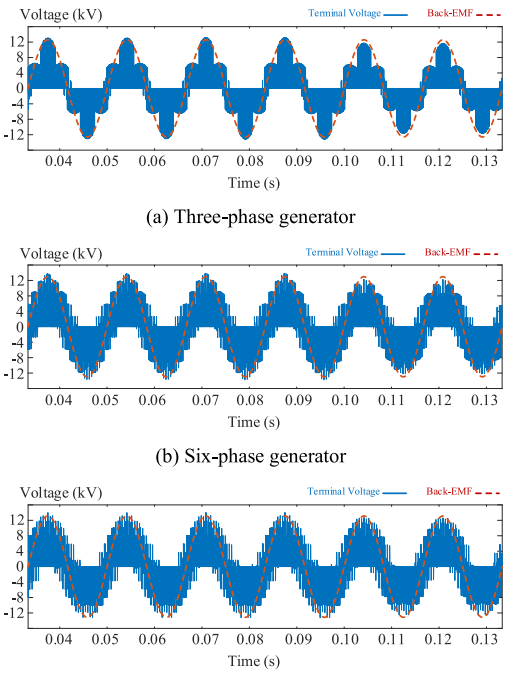

(a) Three-phase generator

(b) Six-phase generator

(c) Nine-phase generator

FIGURE 9. Per-phase back-EMF and voltage waveforms at the terminal of the generator. (a) Three-phase generator. (b) Six-phase generator. (c) Nine-phase generator.

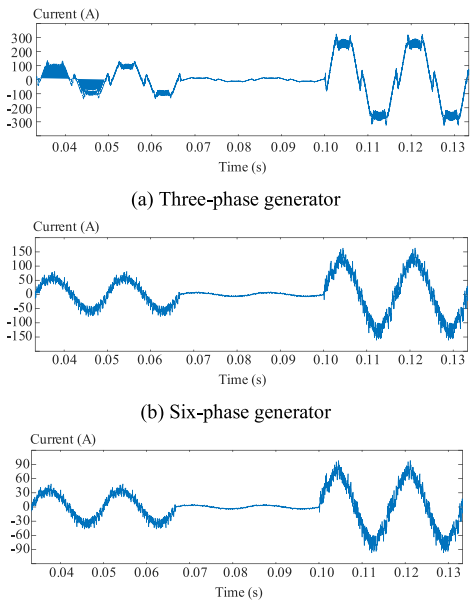

(a) Three-phase generator

(b) Six-phase generator

(c) Nine-phase generator

FIGURE 10. Per-phase current of the generator. (a) Three-phase generator. (b) Six-phase generator. (c) Nine-phase generator.

method results in a significant imbalance across the HVDC-link capacitors, whereas for the other two approaches, the imbalance is notably improved. An important observation is that the MP3L-SVM performs admirably in maintaining a balanced voltage across the capacitors. A slight enhancement

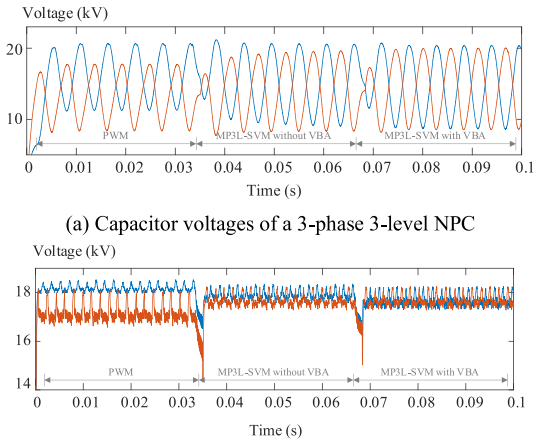

(a) Capacitor voltages of a 3-phase 3-level NPC

(b) Capacitor voltages of a 9-phase 3-level NPC

FIGURE 11. Voltage profile of the HVDC-link capacitors under different control strategies (PWM, SVM without VBA and SVM with VBA). (a) Capacitor voltages of a 3-phase 3-level NPC. (b) Capacitor voltages of a 9-phase 3-level NPC.

is observed with the introduction of the voltage balancing algorithm. This is attributed to the fact that the proposed modulation strategy of MP3L-SVM seeks the three nearest switching states at each stage, ensuring the most optimized switching command. Consequently, the voltages of the capacitors are maintained within a satisfactory range even without the voltage balancing algorithm.

The VBA is designed to address the common challenge in NPC converters related to the fluctuation and imbalance of voltages across the DC-link capacitors. These imbalances can arise due to uneven power distribution, mainly switching irregularities, or load variations, potentially leading to inefficient converter operation, increased stress on components, and reduced lifespan of the system. The switching states of the converter are actively monitored and adjusted by the algorithm to manage the charging and discharging cycles of the capacitors, keeping the voltage across each capacitor within a target range. This is achieved through the careful selection of switching vectors to minimize deviation from the desired voltage levels. In PWM, the switching states are determined by the intersection of the reference voltage and a triangular waveform, making voltage control across the capacitors impossible. Consequently, significant voltage imbalances occur across the capacitors, as shown in Fig. 11. However, in the proposed modulation strategy, the most optimized switching state is selected at each step, inherently balancing the voltage across the capacitors. To further enhance this balance, the strategy integrates the voltage balancing algorithm, ensuring optimal system performance. Fig. 11 demonstrates that the proposed system, even without VBA, performs well in balancing the voltage across the capacitors. Thus, the modulation strategy not only provides a general framework but also significantly reduces voltage imbalance across the capacitors compared to conventional methods such as PWM.

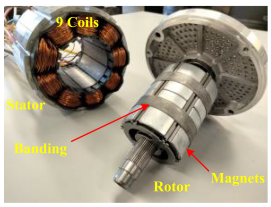

(a) Multiphase generator.

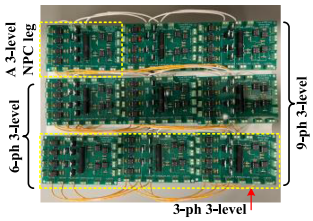

(b) MP3L converter.

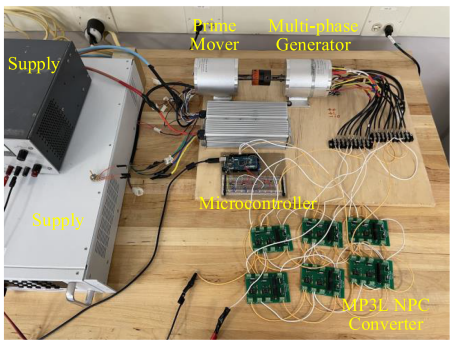

(c) Experimental test setup.

FIGURE 12. Experimental test setup: NPC converter modules, multiphase generator, and test-rig. (a) Multiphase generator. (b) MP3L converter. (c) Experimental test setup.

V. EXPERIMENTAL RESULTS

To validate the simulation results and assess the effectiveness of the MP3L-SVM approach, a laboratory experiment was conducted using a prototype multiphase 3-level NPC converter and a multiphase generator. The generator, depicted in Fig. 12(a), consists of nine concentric coils in the stator, enabling various winding connections such as 3-phase, 6-phase, and 9-phase configurations. The NPC converter is designed in a modular structure, as shown in Fig. 12(b), where each leg is fabricated independently.

The test-rig, illustrated in Fig. 12(c), comprises several components: (1) a 3-level NPC converter, (2) a multiphase generator, (3) a 3-phase permanent magnet motor functioning as a prime mover (wind turbine) for the multiphase generator, (4) a 3-phase inverter to control the prime mover, and (5) the setup also includes a microcontroller, DC power supplies, and monitoring equipment. To evaluate the proposed MP3L-SVM approach, various tests were conducted. Three scenarios, corresponding to the simulation implementation scenarios, are presented: (i) a 3-phase 3-level system, (ii) a 6-phase 3-level system, and (iii) a 9-phase 3-level system. The specifications of the experimental setups are summarized in Table 6.

In the initial phase of the experiments, the generator is configured as a 3-phase generator and connected to three NPC modules, forming a 3-phase 3-level converter. The modulation algorithm is adapted to operate on a microcontroller. During the first stage, the speed of the prime mover is set to be variable, and three scenarios are considered: 700 rpm, 2200 rpm, and 4500 rpm. This setup emulates different wind velocities effectively. Fig. 13(a) displays the rectified voltage for all scenarios. As depicted, the controller swiftly and accurately

TABLE 6. Experimental Test Setup Characteristics

Generator's Number of Phases	3-ph, 6-ph, 9-ph
Number of Coils (Stator)	9 – concentrated coils
Number of Poles	6
Rated Speed (Maximum Speed)	3000 rpm (4500 rpm)
3-phase per-phase RMS back-EMF	30 V
3-phase per-phase peak back-EMF	23 V
Converter's Per-leg Ratings	200 V – 12 A – 2400 W
Switching Frequency	6 kHz

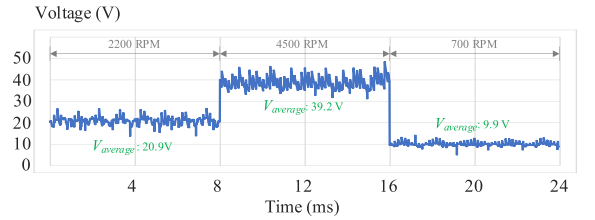

(a) Output DC voltage (variable speed: 2200 rpm – 4500 rpm – 700 rpm)

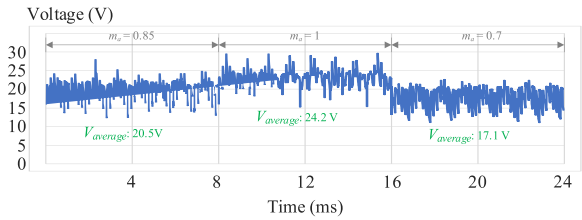

(b) Output DC voltage (variable modulation index: 0.85 – 1.0 – 0.75)

FIGURE 13. First and second stage of the 3-phase 3-level experiments (DC voltage). (a) Output DC voltage (variable speed: 2200 rpm – 4500 rpm – 700 rpm). (b) Output DC voltage (variable modulation index: 0.85 – 1.0 – 0.75).

adjusts itself to variable input without significant transients in all transitions, indicating the exceptional performance of the controller. In the second stage, the generator's speed is fixed at 2200 rpm, and the output voltage is controlled by adjusting the modulation index (m_a). This setup closely simulates real-world scenario, where the wind speed is fixed, and variable output voltage is required. Three modulation indices are considered: 1, 0.85, and 0.7. The converter begins with a modulation index of 0.85, then transitions to 1, followed by 0.75. Fig. 13(b) illustrates the output voltage. It is evident that the controller adeptly adjusts the output voltage based on the desired modulation indices, affirming the controller's robust performance.

In the second phase of the experiments, the generator undergoes reconfiguration as a 6-phase generator and is linked to six NPC modules, thereby constituting a 6-phase 3-level converter. The initial and subsequent stages of the experiments mirror those of the 3-phase configuration. Fig. 14(a) depicts the rectified voltage for variable prime mover speeds, while Fig. 14(b) illustrates the output voltage for different modulation indices. It is evident from the figures that the controller effectively adjusts the output voltage according to the desired modulation indices, thereby affirming the robust performance of the controller for the 6-phase 3-level configuration.

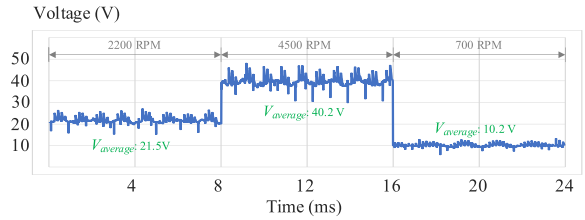

(a) Output DC voltage (variable speed: 2200 rpm – 4500 rpm – 700 rpm)

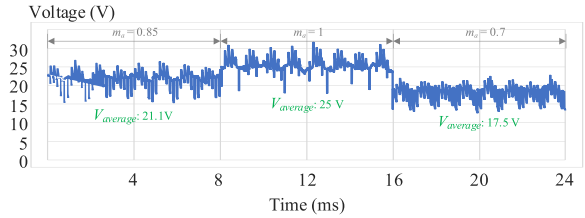

(b) Output DC voltage (variable modulation index: 0.85 – 1.0 – 0.75)

FIGURE 14. First and second stage of the 6-phase 3-level experiments (DC voltage). (a) Output DC voltage (variable speed: 2200 rpm – 4500 rpm – 700 rpm). (b) Output DC voltage (variable modulation index: 0.85 – 1.0 – 0.75).

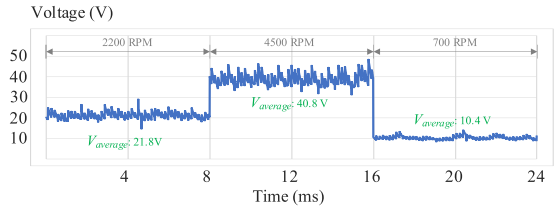

(a) Output DC voltage (variable speed: 2200 rpm – 4500 rpm – 700 rpm)

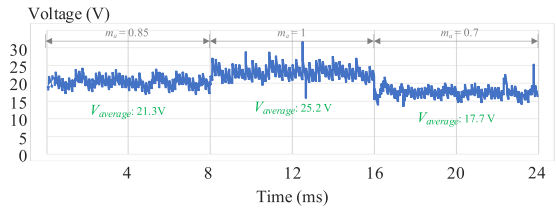

(b) Output DC voltage (variable modulation index: 0.85 – 1.0 – 0.75)

FIGURE 15. First and second stage of the 9-phase 3-level experiments (DC voltage). (a) Output DC voltage (variable speed: 2200 rpm – 4500 rpm – 700 rpm). (b) Output DC voltage (variable modulation index: 0.85 – 1.0 – 0.75).

In the third phase of the experiments, to align with the simulation studies, the generator is reconfigured as a 9-phase generator and connected to nine NPC modules, forming a 9-phase 3-level converter. During the first stage of this experiment, the speed of the prime mover is again set to be variable (700 rpm, 2200 rpm, and 4500 rpm). During the second stage, the generator's speed is fixed at 2200 rpm, and the output voltage is controlled by adjusting the m_a (1, 0.85, and 0.75). Fig. 15(a) presents the rectified voltage for all prime mover's speeds, while Fig. 15(b) illustrates the output voltage for all the mentioned modulation indices. It is evident that the output voltage has increased compared to the same scenarios for 3-phase and 6-phase configurations, while the ripple has reduced.

Additionally, the performance of the controller is exceptional, effectively controlling the output voltage within the desired range. In summary, both simulation and experimental studies demonstrate the effectiveness of the proposed multiphase 3-level general framework for SVM across various numbers of phases and scenarios. Experimental data indicates a consistent increase in rectified voltage with an increasing number of phases, aligning well with simulation results. Moreover, simulations suggest a decrease in the ripple factor of the rectified voltage as the number of phases increases, a trend that is clearly observed in the experimental findings. Additionally, Fig. 16 shows the per-phase AC current of the generator. The switching effect is evident, and it can also be observed that as the number of phases increases, the per-phase current decreases, consistent with the simulation studies.

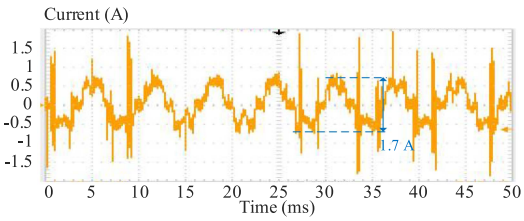

(a) Three-phase generator.

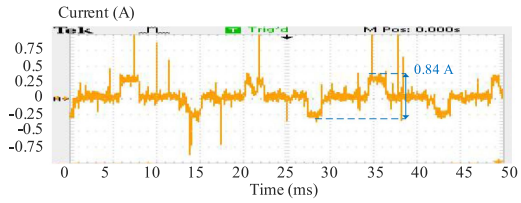

(b) Six-phase generator.

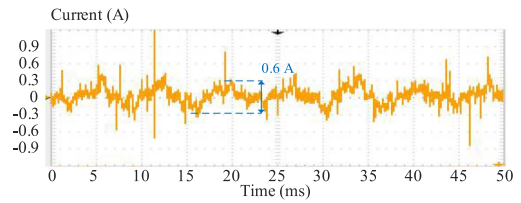

(c) Nine-phase generator.

FIGURE 16. Per-phase AC current of the generator. (a) Three-phase generator. (b) Six-phase generator. (c) Nine-phase generator.

VI. CONCLUSION

This article introduces a multiphase 3-level SVM (MP3L-SVM) strategy for 3-lvvel NPC converters. By employing simplified calculations optimized through an SVD the proposed MP3L-SVM strategy identifies the most efficient switching sequence. The paper also addresses challenges posed by voltage imbalances across the NPC topology's HVDC-link capacitors by integrating a voltage balancing algorithm with the developed modulation strategy. Furthermore, it discusses and implements NPC rectifier challenges within the proposed system. Simulation studies and experimental validation using a scaled-down prototype demonstrate the effectiveness and accuracy of the proposed system and modulation strategy.

REFERENCES

[1] O. Lopez, J. Alvarez, J. Doval-Gandoy, and F. D. Freijedo, "Multilevel multiphase space vector PWM algorithm with switching state redundancy," *IEEE Trans. Ind. Electron.*, vol. 56, no. 3, pp. 792–804, Mar. 2009.

[2] J. Rodríguez, J. S. Lai, and F. Z. Peng, "Multilevel inverters: A survey of topologies, controls, and applications," *IEEE Trans. Ind. Electron.*, vol. 49, no. 4, pp. 724–738, Aug. 2002.

[3] O. Beik and A. Al-Adsani, *DC Wind Generation Systems: Design, Analysis, and Multiphase Turbine Technology*. Berlin, Germany: Springer, 2020.

[4] O. Beik, R. Yang, and A. Emadi, "Design of a 5-phase IPM machine for electric vehicles," in *Proc. IEEE Transp. Electrific. Conf. Expo*, 2018, pp. 168–172.

[5] A. S. Al-Adsani and O. Beik, "Design of a multiphase hybrid permanent magnet generator for series hybrid EV," *IEEE Trans. Energy Convers.*, vol. 33, no. 3, pp. 1499–1507, Sep. 2018.

[6] N. Schofield, X. Niu, and O. Beik, "Multiphase machines for electric vehicle traction," in *Proc. IEEE Transp. Electrific. Conf. Expo*, 2014, pp. 1–6.

[7] O. Beik and A. S. Al-Adsani, "Active and passive control of a dual rotor wind turbine generator for DC grids," *IEEE Access*, vol. 9, pp. 1987–1995, 2021.

[8] J. Rodriguez, S. Bernet, P. K. Steimer, and I. E. Lizama, "A survey on neutral-point-clamped inverters," *IEEE Trans. Ind. Electron.*, vol. 57, no. 7, pp. 2219–2230, Jul. 2010.

[9] R. Dermouche, A. Talaoubrid, L. Barazane, Y. Sellami, M. Tadjine, and N. Zioui, "Qualitative and quantitative analysis of the reliability of NPC and ANPC power converters for aeronautical applications," *Alexandria Eng. J.*, vol. 61, no. 6, pp. 4863–4873, 2022.

[10] O. Beik, A. Dekka, and M. Narimani, "A new modular neutral point clamped converter with space vector modulation control," in *Proc. IEEE Int. Conf. Ind. Technol.*, 2018, pp. 591–595.

[11] A. Dekka, O. Beik, and M. Narimani, "Modulation and voltage balancing of a five-level series-connected multilevel inverter with reduced isolated direct current sources," *IEEE Trans. Ind. Electron.*, vol. 67, no. 10, pp. 8219–8230, 2019.

[12] N. P. Schibli, T. Nguyen, and A. C. Rufer, "A three-phase multilevel converter for high-power induction motors," *IEEE Trans. Power Electron.*, vol. 13, no. 5, pp. 978–986, Sep. 1998.

[13] M. S. A. Dahidah and V. G. Agelidis, "Selective harmonic elimination PWM control for cascaded multilevel voltage source converters: A generalized formula," *IEEE Trans. Power Electron.*, vol. 23, no. 4, pp. 1620–1630, Jul. 2008.

[14] J. F. Silva, N. Rodrigues, and J. Costa, "Space vector alpha-beta sliding mode current controllers for three-phase multilevel inverters," in *Proc. IEEE 31st Annu. Power Electron. Specialists Conf.*, 2000, pp. 133–138.

[15] J. D. Barros and J. F. Silva, "Optimal predictive control of three-phase NPC multilevel converter for power quality applications," *IEEE Trans. Ind. Electron.*, vol. 55, no. 10, pp. 3670–3681, Oct. 2008.

[16] J. Kolb, F. Kammerer, and M. Braun, "Straight forward vector control of the modular multilevel converter for feeding three-phase machines over their complete frequency range," in *Proc. 37th Annu. Conf. IEEE Ind. Electron. Soc.*, 2011, pp. 1596–1601.

[17] A. Bakeer, I. S. Mohamed, P. B. Malidarreh, I. Hattabi, and L. Liu, "An artificial neural network-based model predictive control for three-phase flying capacitor multilevel inverter," *IEEE Access*, vol. 10, pp. 70305–70316, 2022.

[18] M. R. Homaeinezhad, M. Homaeinezhad, S. Akbari, and D. N. G. Hosseini, "Input-decoupled discrete-time sliding mode control algorithm for servo multi-field multi-armature DC machine," *ISA Trans.*, vol. 127, pp. 283–298, 2022.

[19] S. Yaqubi, M. Homaeinezhad, and M. R. Homaeinezhad, "Adaptive fuzzy-wavelet neural networks-based real-time model generation for increasing tracking precision of multivariable servo actuator," *Mechatron. Syst. Control*, vol. 50, no. 1, pp. 1–6, 2022.

[20] N. Celanovic and D. Boroyevich, "A fast space-vector modulation algorithm for multilevel three-phase converters," *IEEE Trans. Ind. Appl.*, vol. 37, no. 2, pp. 637–641, Mar./Apr. 2001.

[21] M. M. Prats, L. G. Franquelo, R. Portillo, J. I. León, E. Galván, and J. M. Carrasco, "A 3-D space vector modulation generalized algorithm for multilevel converters," *IEEE Power Electron. Lett.*, vol. 1, no. 4, pp. 110–114, Dec. 2003.

[22] J. I. Leon, R. Portillo, L. G. Franquelo, S. Vazquez, J. M. Carrasco, and E. Dominguez, "New space vector modulation technique for single-phase multilevel converters," in *Proc. IEEE Int. Symp. Ind. Electron.*, 2007, pp. 617–622.

[23] L. Gao and J. E. Fletcher, "A space vector switching strategy for three-level five-phase inverter drives," *IEEE Trans. Ind. Electron.*, vol. 57, no. 7, pp. 2332–2343, Jul. 2010.

[24] O. Dordevic, M. Jones, and E. Levi, "A comparison of PWM techniques for three-level five-phase voltage source inverters," in *Proc. 14th Eur. Conf. Power Electron. Appl.*, 2011, pp. 1–10.

[25] E. A. R. Engku Ariff, O. Dordevic, M. Jones, and E. Levi, "Space vector PWM technique for a three-level asymmetrical six-phase drive," in *Proc. 8th Int. Eng. Technol. Int. Conf. Power Electron., Machines Drives*, 2016, pp. 1–6.

[26] O. Dordevic, E. Levi, and M. Jones, "A vector space decomposition based space vector PWM algorithm for a three-level seven-phase voltage source inverter," *IEEE Trans. Power Electron.*, vol. 28, no. 2, pp. 637–649, Feb. 2013.

[27] J. I. Leon et al., "Multilevel multiphase feedforward space-vector modulation technique," *IEEE Trans. Ind. Electron.*, vol. 57, no. 6, pp. 2066–2075, Jun. 2010.

[28] Ó. López et al., "Carrier-based PWM equivalent to multilevel multiphase space vector PWM techniques," *IEEE Trans. Ind. Electron.*, vol. 67, no. 7, pp. 5220–5231, Jul. 2020.

[29] M. Homaeinezhad and O. Beik, "Active and passive control of nine-phase wind turbine conversion systems : A comparison," in *Proc. IEEE Int. Electric Machines Drives Conf.*, 2023, pp. 1–7.

[30] M. Homaeinezhad, O. Beik, and A. Karni, "Multiphase multilevel NPC converter for MVDC electric ship applications," in *Proc. IEEE Electric Ship Technol. Symp.*, 2023, pp. 121–128.

[31] M. Homaeinezhad and O. Beik, "Modified space vector modulation and voltage balancing of multiphase neutral point clamped rectifier," in *Proc. IEEE Energy Convers. Congr. Expo.*, 2023, pp. 3422–3428.

[32] M. Homaeinezhad, O. Beik, and A. Karni, "Reliability considerations for large spacecraft propulsion system," in *Proc. IEEE Aerosp. Conf.*, 2024, pp. 1–11.

[33] O. Beik, "An HVDC off-shore wind generation scheme with high voltage hybrid generator," Ph.D. dissertation, Dept. Electr. Comp. Eng., McMaster Univ., Hamilton, ON, Canada, 2016.

[34] A. S. Al-Adsani and O. Beik, "Characterization of a hybrid PM generator using a 32-phase brushless excitation scheme," *IEEE Trans. Energy Convers.*, vol. 34, no. 3, pp. 1391–1400, Sep. 2019.

[35] M. Saeedifard, R. Iravani, and J. Pou, "Analysis and control of DC-capacitor-voltage-drift phenomenon of a passive front-end five-level converter," *IEEE Trans. Ind. Electron.*, vol. 54, no. 6, pp. 3255–3266, Dec. 2007.

[36] A. Dekka, O. Beik, and M. Narimani, "Modulation and voltage balancing of a five-level series-connected multilevel inverter with reduced isolated direct current sources," *IEEE Trans. Ind. Electron.*, vol. 67, no. 10, pp. 8219–8230, Oct. 2020.